CRYSTAL GROWTH & DESIGN

pubs.acs.org/crystal

Article

Role of Specific and Nonspecific Interactions in the Crystallization Behavior of BSA and HSA Protein Solutions

Maximilian D. Senft,* Georg Zocher,* Sebastian Retzbach, Ralph Maier, Anusha Hiremath, Fajun Zhang,* Thilo Stehle, and Frank Schreiber

Cite This: *Cryst. Growth Des.* 2025, 25, 2418−2429

Read Online

ACCESS | Metrics & More | Article Recommendations | Supporting Information

ABSTRACT: The crystallization conditions of proteins are sensitive to the prevailing interactions. Even the two similar proteins, bovine and human serum albumin (BSA and HSA), exhibit different crystallization conditions despite their comparable function, biophysical properties, shape, and size (≈60 kDa and a 75.8% sequence identity). In this work, we provide a comparison of specific and nonspecific interactions regarding the crystallization behavior of BSA and HSA. The results of the analysis of crystal packing interfaces indicate that HSA uses a relatively larger part of its surface area to establish crystal contacts compared to its bovine counterpart. Likewise, HSA utilizes more of its residues for crystal contact formation, offering a broader range of options to establish attractive interactions. Phase diagrams of the BSA−PEG and HSA−PEG systems were established in order to gain more precise insights into the nonspecific depletion interactions. It turns out that BSA crystallizes predominantly via depletion interactions, whereas HSA does not. Subsequent systematic small-angle scattering (SAXS) measurements of the two systems in combination with quantitative modeling provide insights into the induced effective interactions, allowing for a better understanding of the two protein−PEG systems. The results obtained were compared to the previously established reentrant condensation (RC) phase behavior of BSA and HSA. The RC phase behavior is caused by the specific interaction of proteins with added multivalent cations. In this case, HSA crystallizes, but BSA does not. This comparison emphasizes the different roles of specific and nonspecific interactions for the crystallization behavior of BSA and HSA.

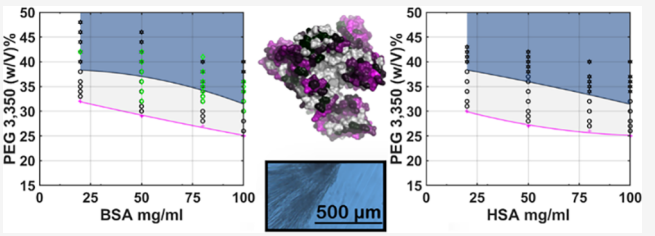

INTRODUCTION

Understanding the effective interactions of proteins requires sound knowledge of the basic thermodynamic properties of the protein solution, ranging from concentration to solvent properties. Solvent properties include pH value, ionic strength, and the properties of the additives.[1−3] The resulting effective interactions between protein molecules can be tuned by the addition of salts, polymers,[3−5] or small organic molecules,[3] thus influencing the phase behavior. Protein phase diagrams enable predictions,[6] contributing to the study of protein condensation-related[7−10] and crystallization-related diseases.[11−15]

Previous work on bovine serum albumin (BSA) and human serum albumin (HSA) in the presence of trivalent metal salts such as YCl_3 or $CeCl_3$ showed that both proteins feature a rich and diverse phase behavior.[16−18] Moreover, the results showed that HSA crystallized reliably under the experimental conditions used, whereas BSA did not.[17] This approach exploits specific interactions[19] to induce the rich phase behavior of the two proteins and the crystallization of HSA.[17,18] This different crystallization behavior is particularly interesting, as both proteins share numerous similarities and perform similar tasks in their respective mammalian species. Mammalian serum albumin is not only responsible for the binding and transportation of small molecules, such as fatty acids or amino acids, but also for physiological functions, including the maintenance of the pH value and the osmotic pressure of the blood plasma.[20−22] Apart from that, they share a comparable size and 75.8% sequence identity.[23] Despite these similarities, upon examination of the physiochemical properties, which are summarized in Table 1, subtle differences are apparent as well and are frequently not sufficiently taken into account. The industrial production of BSA is cheaper and more convenient than its homologous human counterpart, which is why BSA is often examined as a reference for globular proteins, and the results are thus assigned to HSA.[24] Further analogies, characteristics, and differences of the two proteins BSA and HSA are discussed in detail in ref 17.

Taking these subtle differences into account, aqueous BSA and HSA protein solutions were exposed to the nonspecific, polymer-induced depletion interaction to elucidate the role of

Received: November 8, 2024
Revised: March 10, 2025
Accepted: March 11, 2025
Published: March 26, 2025

Table 1. Important Physiochemical Properties of BSA and HSA

	BSA	HSA
# amino acid	583[77]	585[20]
molecular weight [kDa]	66.4−67[78,79]	66.4−69[20,80]
pI	4.6[25]	4.7[20]
specific volume [mL/g]	0.735[81]	0.754[82]
ellipsoid $R(a)$ [Å]	17	18
ellipsoid $R(b)$ [Å]	42.00−55.00	45.00−56.17
extinction coefficient [mL × mg^{-1} × cm^{-1}]	0.667[83]	0.531[83]

specific and nonspecific interactions in phase and crystallization behavior. In a colloidal context, HSA and BSA exhibit a globular structure combined with a net negatively charged surface at neutral pH.[25] In order to describe the present system, proteins are interpreted as spheres that exhibit (essentially) hard-sphere interactions. Synthetic polymers, on the other hand, are regarded as penetrable hard spheres that do not interact with each other. Each protein is surrounded by a depletion layer. Once two depletion layers overlap, a previously inaccessible volume becomes available for the polymer chains, causing an entropy gain. The overlap of depletion layers entails that no polymer can remain nor enter this area, yielding an attractive force pushing the proteins together.[26,27] This attractive force results exclusively from repulsive interactions originating from the entropic effect.[27−30] Yet, two distinct cases result from the size differences between proteins and polymers, referred to as the protein limit[31−33] and the colloid limit.[28−30] In the colloid limit, the polymer chains are smaller than or similar in size to the proteins, whereas the protein limit describes the opposite case.[28−33] Apart from depletion interactions, a direct interaction between polymers and proteins is postulated.[34,35] Even though polyether[36] PEG is regarded as an unbranched, nonionic, nonadsorbing polymer ($H(OCH_2CH_2)nOH$),[37] interactions between polymers and proteins via hydrogen bond formation cannot be ruled out.[38] This results in interactions that are more complicated than those exclusively responsible for depletion.

In this work, we investigated the depletion-induced effects of polymer PEG on the phase behavior of proteins BSA and HSA. In addition to the macroscopic phase behavior, systematic small-angle X-ray scattering (SAXS) experiments within the colloidal limit while exceeding the overlap concentration of the polymer (c^*) provide further insight into the effective interactions. Fitting the SAXS data with a sticky hard-sphere potential allows for the characterization of the prevailing effective interactions. The results obtained, which are attributable to nonspecific depletion effects, were compared with the reentrant condensation (RC)[39] phase behavior induced by specifically acting metal cations.[19] It was shown that YCl_3 and $CeCl_3$ induce RC phase behavior for both proteins, while crystallization only occurred for HSA.[16−18] However, if the effect is changed from specific interactions (metal cations) to nonspecific interactions (PEG-induced depletion), only BSA crystals form. The unit cell parameters of BSA crystals were determined by X-ray diffraction analysis. A comparison of the crystal structure with the literature[23,40] was not only limited to BSA but also extended to HSA. By sophisticated purification and labor-intensive protocols, HSA crystallization was reported to occur in the presence of PEG.[22,41] Analyzing these crystal structures offers new insights into effective protein−protein interactions and their tunability by selecting specific or nonspecific interactions. The experimental results underline the importance of the chosen crystallization strategy, as the subtle differences between the two similar proteins, BSA and HSA, are not negligible.

RESULTS AND DISCUSSION

Phase Behavior of BSA and HSA in the Presence of PEG. Initially, experimental phase diagrams for both proteins, BSA (Figure 1(a)) and HSA (Figure 1(b)), in the presence of 100 mM NaCl with increasing (w/V)% ratios of PEG (0−45 (w/V)%) at RT (21 ± 1 °C) were established by macroscopic inspection combined with microscopy. The protein concentration was varied between 20, 50, 80, and 100 mg/mL. Both proteins feature a rich phase behavior, which includes liquid−liquid phase separation (LLPS), aggregation, and, for BSA, crystallization (see Figure 1(a,b), respectively). Due to the admixing of 100 mM NaCl, the charges of the globular, negatively charged proteins BSA and HSA are screened. The solutions appeared macroscopically clear upon visual inspection (see Figure 1(c) for BSA and Figure 1(d) for HSA). Further increase of the PEG concentration ((w/V)%) resulted in a visually opaque solution. This transition from clear to opaque is named t^* and highlighted by a magenta line for the two respective plots (see Figure 1(a) for BSA and Figure 1(b) for HSA).

In addition to the visual inspection, microscopic images were taken to support the macroscopic observations (see panels (a)−(c) in Figure 2 for BSA and panels (d)−(f) in Figure 2 for HSA). Analysis of both phase diagrams revealed that both proteins feature a comparable t^* transition, where lower protein amounts require higher concentrations of PEG to derive the system in a turbid state. For BSA at 20 mg/mL, this transition occurs at 33 (w/V)% PEG, while for 20 mg/mL HSA, it occurs at 30 (w/V)% PEG. At 100 mg/mL, both proteins feature a similar t^* transition point at 25 (w/V)% PEG. For both proteins, LLPS occurs just above the t^* transition. Noteworthy, more LLPS conditions were found for HSA, resulting in a larger area of the phase diagram being occupied by LLPS compared to BSA (see the grayish areas in Figure 1(a,b)). Generally, lower concentrations of the respective protein require higher PEG concentrations to induce LLPS.

Above the LLPS threshold (at very high PEG concentrations), aggregate formation is found for both proteins. However, the phase behavior of BSA differs significantly from that of HSA due to crystal formation (see Figure 1(a) green diamonds and Figure 2 microscopic image (c)). Notably, crystallization was observed under additional conditions (data not shown). A comparison of the HSA phase diagram with the BSA phase diagram shows a shift in LLPS toward higher PEG concentrations ((w/V)%) for BSA, while the phase boundary t^* is also slightly shifted upward. This indicates stronger attractions in HSA than in BSA solutions under the same conditions, particularly below or at the transition t^* (see Figure 5).

Visual inspection was performed immediately after sample preparation. The samples were prepared in one set, i.e., one protein concentration (e.g., 50 mg/mL) with increasing PEG 3350 concentrations at a constant level of 100 mM NaCl. Visual inspection images (see Figure 1(c),(d)) were taken immediately after sample preparation (within a minute to hour timescale). Microscopy images (see Figure 2(a−f)) were acquired after sample preparation (within 1 or 2 days).

https://doi.org/10.1021/acs.cgd.4c01535
Cryst. Growth Des. 2025, 25, 2418−2429

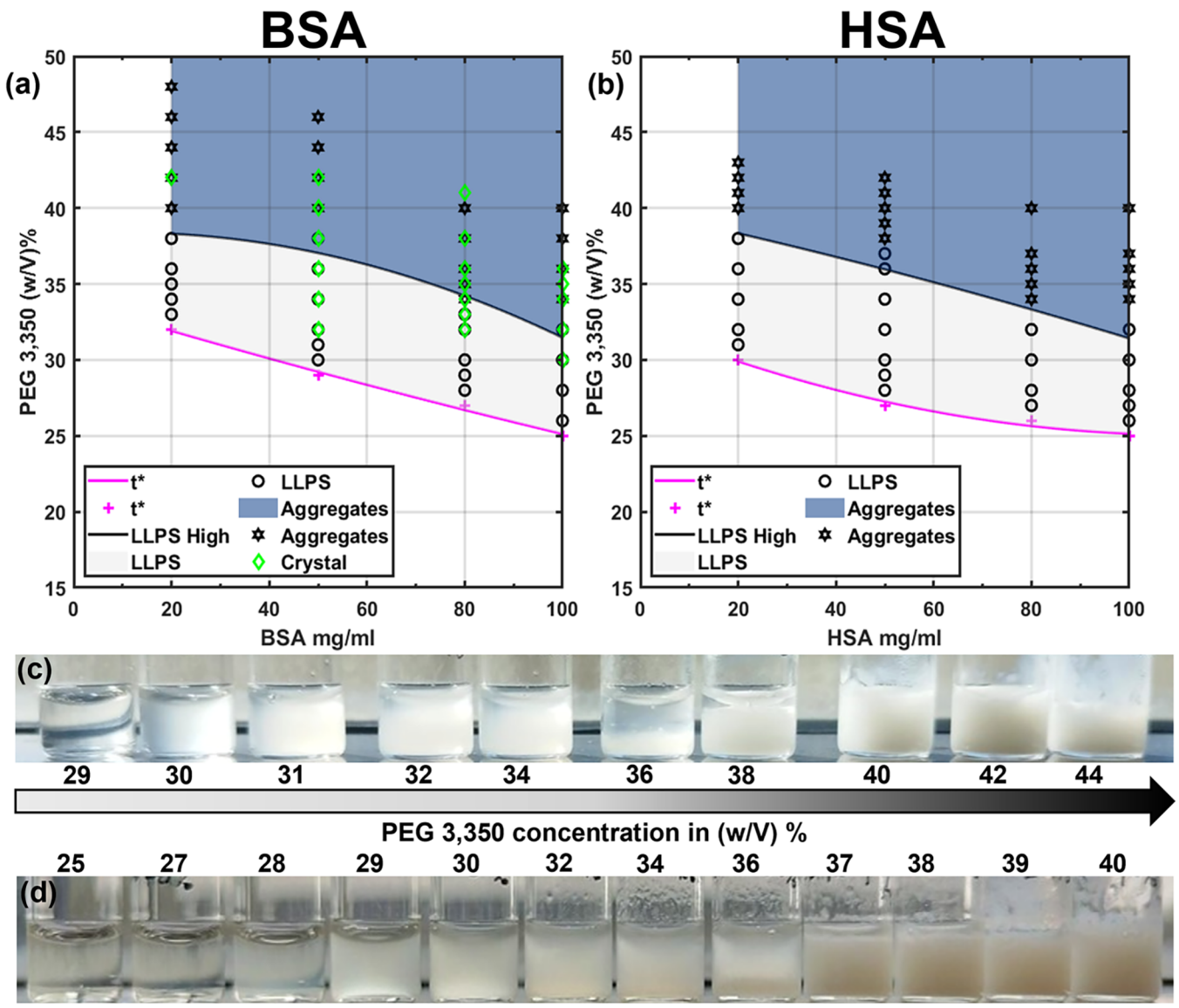

Figure 1. Phase behavior of (a) BSA and (b) HSA at protein concentrations of 20, 50, 80, and 100 mg/mL, in the presence of 100 mM NaCl, with increasing amounts of (w/V)% of PEG M_w 3350. The phase transition t^* is highlighted by a magenta line. LLPS is to be observed within the gray-shaded area. Black solid lines show the respective LLPS border. Aggregates are observed within the blue-shaded area. For BSA, (a) green triangles marked crystal formation. Black stars and black circles show the investigated samples featuring aggregates and LLPS, respectively (a, b). In (c), a photograph shows the visual inspection of BSA at a concentration of 50 mg/mL, admixed with increasing (w/V)% of PEG (from 29 to 44 (w/V)%), arranged from left to right. In (d), a photograph shows the visual inspection of HSA at a concentration of 50 mg/mL, admixed with increasing (w/V)% of PEG (from 25 to 40 (w/V)%), also arranged from left to right. Photographs (c, d) were taken immediately after sample preparation (minute to hour timescale).

However, microscopy images of BSA protein crystals (Figure 2(c)) were taken after growth. BSA crystallization was observed after incubating for a few days (up to 7 days). Further incubation of crystalline samples (from 7 days up to a month) promoted crystal growth but did not necessarily enhance the growth of quality crystals. It was observed that after a long enough period of time (individual for each crystalline sample), the crystals appeared enlarged and submerged in a translucent liquid.

Incubation beyond 2 days enhanced aggregate sedimentation and promoted the formation of a dense white sludge buildup at the bottom of the reaction vail for samples featuring LLPS and aggregates. The small liquid phase above this dense white sludge remained clear and translucent.

Size Ratio q and Colloidal Limit. To ensure the applicability of the depletion effect, the length scales of the polymer solutions, which were changed by increasing or decreasing the polymer concentration ((w/V)%), had to be assessed to capture the interaction between the proteins. Given a dilute system, the radius of gyration (eq 1) of the polymer provides an estimate of the applicable length scales[42]

$$R_{g,PEG} = 0.0215 M_w^{(0.583\pm0.031)} \quad (1)$$

where M_w denotes the average molecular weight. Due to shrinkage of the PEG polymer chain with increasing concentration,[43] the radius of gyration needs to be adjusted according to eq 2.[44]

https://doi.org/10.1021/acs.cgd.4c01535
Cryst. Growth Des. 2025, 25, 2418−2429

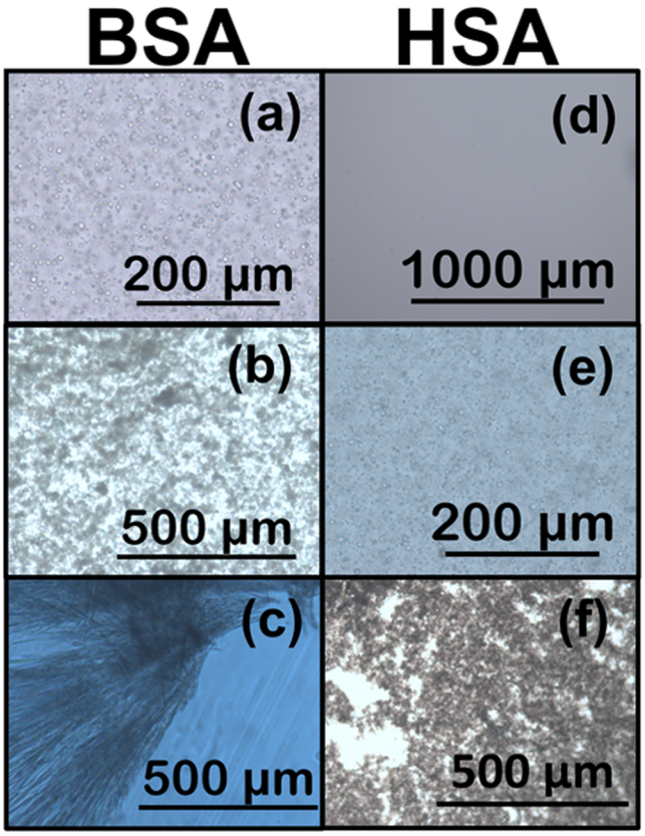

Figure 2. Microscopic examination of (a–c) BSA and (d–f) HSA. All microscopic images share a protein concentration of 50 mg/mL mixed with 100 mM NaCl. Panel (a) shows a snapshot of LLPS for BSA at 30 (w/V)% PEG. Representative microscopic snapshots of (b) BSA aggregation at 40 (w/V)% PEG, (c) BSA crystal at 34 (w/V)% PEG, (d) below t^* for HSA at 26 (w/V)% PEG, (e) LLPS for HSA at 32 (w/V)% PEG, and (f) HSA aggregation at 41 (w/V)% PEG.

$$R_{G,PEG} = R_{g,PEG}(c_{PEG}/c^*_{PEG})^{-1/8} \quad (2)$$

Upon reaching the overlap concentration c^* of the polymer, the solution is referred to as semidilute.[45] At c^*, the polymer chains start to overlap, forming an entangled polymer mesh.[46] In the case of PEG 3350, c^* can be found at 10 (w/V)%.[47] Here, the radius of gyration inadequately describes the applicable length scales. Therefore, the length scale has to be adjusted to the polymer mesh size ζ_b.[42,48] This mesh size can be calculated using eq 3.[44]

$$\zeta_b \approx R_{G,PEG,}(c_{PEG}/c^*_{PEG})^{-3/4} \quad (3)$$

Based on this formula (eqs 1, 2, and 3), the size ratio q (eq 4)[32] for both BSA and HSA proteins at 50 and 100 mg/mL in the presence of 100 mM NaCl with increasing PEG (w/V)% can be obtained (see Figure 3).

$$q = \frac{2\zeta_b}{\sigma} \quad (4)$$

Here, the diameter of the respective protein is denoted by σ. This size ratio q allows the classification of the colloid polymer solutions into different categories. If the size ratio $q < 1$ is applicable, this is referred to as the colloidal limit, whereas in the opposite case, $q > 1$ is classified as the protein limit.[27,31,32,45] The experiments shown in this work are within the colloidal limit (see Figure 3). In addition to a size ratio of

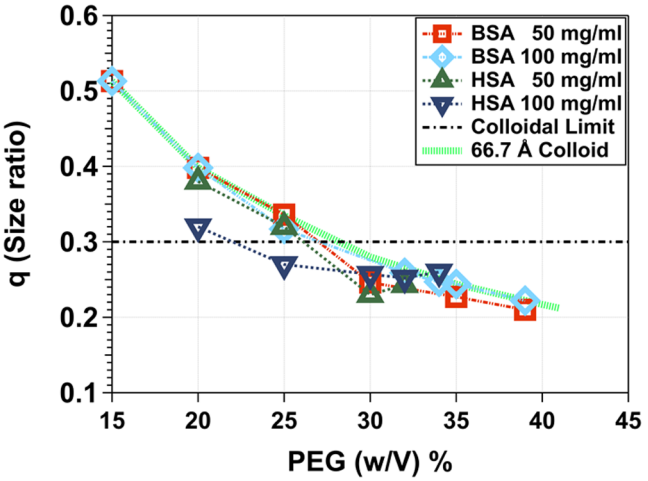

Figure 3. Calculated size ratio q for 50 and 100 mg/mL BSA and HSA in the presence of 100 mM NaCl for different PEG concentrations ((w/V)%). The black dashed line indicates the theoretically determined colloidal limit. The green line serves as a guide to the eye and indicates the size ratio for a colloid with a diameter σ of 66.7 Å. Besides, lines serve as guides to the eye.

$q < 1$, the requirement of $q < 0.3$ was met for most conditions, which allows for an area of coexistence between a colloidal crystal and liquid (strictly for $q < 0.3$) as well as some form of gas–liquid coexistence ($q > 0.3$) within the phase diagram.[27,31,32,49−51]

Based on the formalism shown above, the size ratio q is the largest around the overlap concentration c^*. The experiments reported here are in the q range from $q \approx 0.55$ to $q \approx 0.2$. The black dashed line in Figure 3 indicates the aforementioned condition of $q < 0.3$, above which gas–liquid-type coexistence can be found. This agrees with the experimentally determined phase diagrams (see Figure 1(a),(c)). On the other hand, below this line, crystal formation and coexistence of a colloidal crystal and liquid is possible. It was found that the crystallization conditions for BSA are in agreement with this experimentally and theoretically determined limit (see also Figures 1(a) and 2(c)) for the reported experiments. Therefore, the rich phase behavior observed here can be described as a consequence of the depletion effect.

Depletion-Induced Effective Protein–Protein Interactions. In order to obtain further information about the effective protein–protein interactions upon the addition of PEG M_w 3350, systematic SAXS measurements were performed. The obtained results for protein concentrations of 50 and 100 mg/mL BSA and HSA admixed with 100 mM NaCl are summarized in Figure 4. At low PEG concentrations, all SAXS curves share a common feature: with increasing PEG concentration, the intensity at low Q increases. This initial increase can be equated to a reduction of repulsion. A further increase in the PEG concentration yields an attraction, with the low Q intensity reaching its maximum. For 50 mg/mL BSA and HSA, the maximum can be observed at 30 (w/V)% PEG (see Figure 4(a),(c)). For 100 mg/mL BSA and HSA, the maximum is visible at 25 (w/V)% PEG (see Figure 4(b),(d)).

Further increase in the PEG concentration yields LLPS (see Figure 1(a),(b)) and leads to a low Q decrease (see Figure 4). Curves for 50 mg/mL BSA with 35 and 39 (w/V)% PEG (see Figure 4(a)) and 100 mg/mL BSA with 39 (w/V)% PEG (see Figure 4(b)) feature a different shape for low and intermediate

https://doi.org/10.1021/acs.cgd.4c01535
Cryst. Growth Des. 2025, 25, 2418−2429

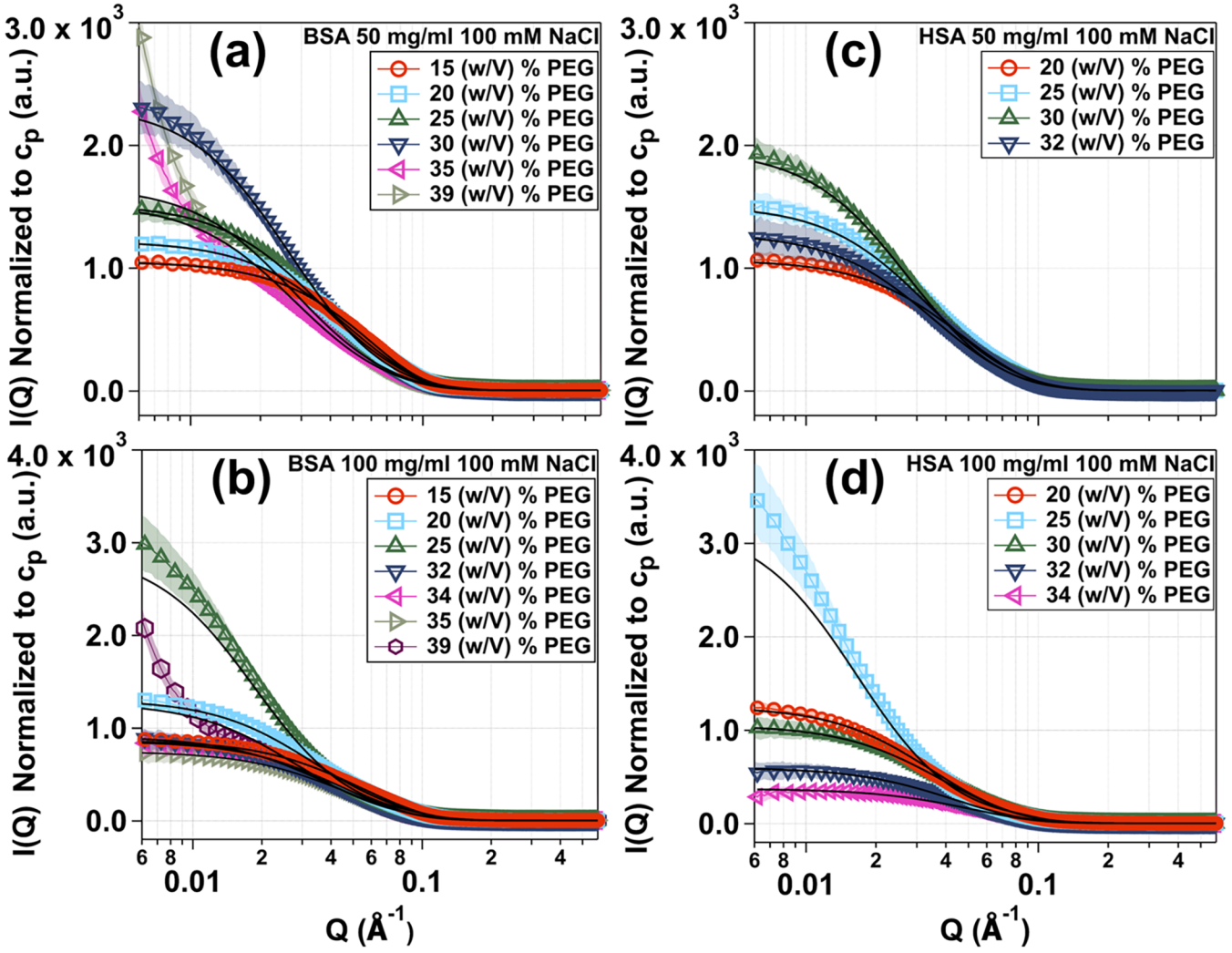

Figure 4. SAXS data for 50 mg/mL (a, c) and 100 mg/mL (b, d) BSA/HSA in the presence of 100 mM NaCl. Data are background-corrected and normalized to the respective protein concentration (c_p). Due to phase separation and aggregation, the SAXS measurements were performed on the dilute phase of the respective samples. In order to ensure comparability, the resulting SAXS intensity profiles were normalized to the original protein concentration using a control sample. Further details on normalization to the protein concentration c_p can be found in the Experimental Section. Throughout, the PEG concentration (w/V)% varies from 15 to 39%. SHS model fits are featured as a solid black line. For readability, only every fifth data point is shown. Besides the black line (SHS model fit), lines serve as guides for the eye. Note that the error bars are represented as opaque shadows with the corresponding color.

Q, compared to the other curves of their respective sample sets. This behavior can be traced back to BSA condensate/aggregate formation. An ellipsoidal form factor combined with an SHS model (solid black lines) was applied as a model to fit the data. Based on these fits, B_2/B_2^{HS} values were extracted, which allow for quantifying these aforementioned observations. B_2/B_2^{HS} values can be termed an intermolecular measure of interactions. The prefixes of the B_2/B_2^{HS} values indicate the type of interaction; i.e., values greater than zero indicate net repulsion, whereas values less than zero indicate net attraction. All investigated samples (Figure 5), regardless of the protein system (BSA or HSA), feature an initial B_2/B_2^{HS} value around ±0.0, indicating neutral to attractive intermolecular interactions. With increasing PEG concentration (w/V)%, the B_2/B_2^{HS} curves decrease linearly before reaching a common B_2/B_2^{HS} value of ≈−1.5 at 25 (w/V)% PEG.

At a concentration of 25 (w/V)% PEG, the value of B_2/B_2^{HS} is lower for HSA than for BSA. This is consistent with the phase diagrams (see Figure 1(a),(b)) and indicates stronger attractive forces in HSA than in BSA solutions under the same conditions (25 (w/V)% PEG). However, a further increase in the PEG (w/V)% concentration leads to a reversal of this effect, which is reflected in lower B_2/B_2^{HS} values for BSA than for HSA (see Figure 5(a)).

Beyond 25 (w/V)%, the curves for 50 and 100 mg/mL HSA likewise decrease linearly, albeit with a less pronounced slope. The same tendency can be seen for 100 mg/mL BSA. Only the curve for 50 mg/mL BSA is different. This curve decreases linearly up to 35 (w/V)% PEG. Above 35 (w/V)% PEG, the slope changes and becomes steeper before reaching its minima at = −3.5 B_2/B_2^{HS}. The B_2/B_2^{HS} curves are in good agreement with the experimentally obtained phase diagrams (see Figure 1(a),(b)). A deeper analysis of the collected data (Figures 1, 3, and 4) indicates that the observed crystallization conditions of BSA occur in the predicted q range of $q < 0.3$, which allows the coexistence of a colloidal crystal and colloidal liquid. This behavior is in accordance with the literature.[27,31,32,49−51] Similarly, the occurrence of crystals can be characterized by

https://doi.org/10.1021/acs.cgd.4c01535
Cryst. Growth Des. 2025, 25, 2418−2429

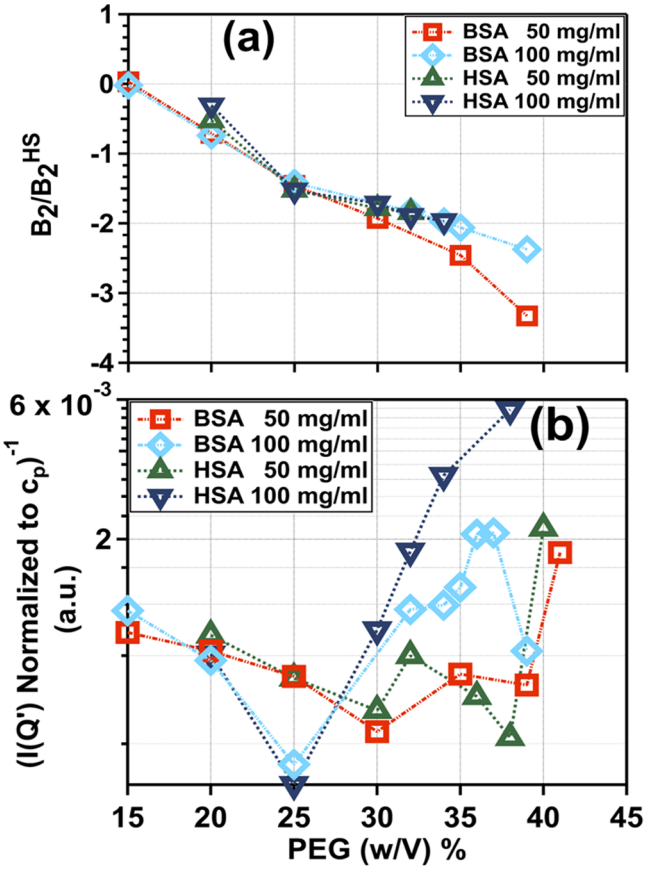

Figure 5. (a) Reduced second virial coefficients and (b) $1/(I(Q')$ normalized to $c_p \to 0)$ behavior of BSA and HSA at 50 and 100 mg/mL in the presence of 100 mM NaCl as a function of PEG (w/V)% concentration. (b) Due to phase separation and aggregation, SAXS measurements were performed with the dilute phase of the respective samples. In order to ensure comparability, the resulting SAXS intensity profiles were normalized to the original protein concentration using a control sample. Further details on normalization to the protein concentration c_p can be found in the Experimental Section. For BSA (50 mg/mL) with 35 and 40 (w/V)% PEG and HSA (100 mg/mL) with 39 (w/V)% PEG, the respective fits (see Figure 4) were used to extract the inverse intensities (further details are provided in the text). The inverse intensity was evaluated at $Q' = 0.0064$ Å^{-1}. The dashed lines in (a, b) serve as guides for the eye. The respective error values are smaller than the markers used and are not plotted for readability.

a window of B_2/B_2^{HS} values: $-10 \lesssim B_2/B_2^{HS} \lesssim -1$,[52−54] which is well consistent with the data shown here.

Moreover, a model-free analysis of the inverse intensity $1/(I(Q')$ normalized to $c_p \to 0)$ of the scattering at low Q values ($Q' = 0.0064$ Å^{-1}), close to the origin, was performed (Figure 5(b)). Unlike the model-based SHS analysis, this method does not require attractive conditions within the system. This approach is connected to the reduced second virial coefficient shown by the following relation.[55−57]

$$\frac{1}{I(Q \to 0)} \propto \frac{1}{S(Q \to 0)} = 1 + 2B_2\rho + \ldots \quad (5)$$

If LLPS is absent, the protein concentration c_p can be expressed to be proportional to the number density ρ ($c_p \propto \rho$), so the inverse intensity $1/I(Q \to 0)$ is proportional to the reduced second virial coefficient. Due to the occurrence of LLPS, c_p varies between the measured dilute and the dense phase, leading to the differences that are to be seen when comparing B_2 with $1/I(Q \to 0)$.

Importantly, for the matching dilute and dense phase, the same reduced values of the second virial coefficient can be obtained as a result of phase equilibrium.[53,58,59] The results presented for protein interactions are in agreement with macroscopic observations (Figures 1 and 5). All samples feature LLPS and show an initial decrease in the inverse intensity followed by an increase after reaching the respective minima. This behavior is in accordance with the second virial coefficient analysis. Looking at the inverse intensity, two different minima are observed. Curves for 100 mg/mL BSA and HSA feature a minima at 25 (w/V)% PEG, whereas for curves of 50 mg/mL BSA and HSA, this minima occurs at higher PEG concentrations (30 (w/V)%). Increasing the PEG concentration further results in an LLPS, perceived as an inverse intensity increase. Due to the low Q increase at 50 mg/mL BSA with 35 and 39 (w/V)% PEG and 100 mg/mL BSA with 39 (w/V)% PEG induced by BSA aggregation/condensation, the corresponding SHS model fit was used for the inverse intensity (see Figures 4(a),(b) and 5(b)). The fit does not consider aggregation, yielding a curve following a pattern similar to that without aggregation. Note that generally we assume an uncertainty of 10% for the SAXS results presented here, which arise from preparatory inaccuracies and data collection.

In order to elucidate the differences between nonspecific and specific interactions with regard to the crystallization behavior of BSA and HSA, the results obtained for nonspecific interactions are compared to those from previous studies on BSA and HSA in the presence of trivalent metal salts. Examining BSA and HSA in the presence of trivalent salts yields a rich and diverse phase diagram, comparable to that observed in the depletion interaction (Figure 1). It is known that trivalent salts induce reentrant condensation (RC) phase behavior in HSA and BSA solutions.[16−18,39,60,61] The rich and diverse phase diagram of RC not only contains aggregates but also shows LLPS or crystallization.[17−19,25,39,62,63] Initially, the protein molecules possess a net negative surface charge and repel each other.[16,39,60,63−65] In addition, the long-range electrostatic repulsion stabilizes the protein molecules, and the solution appears clear.[39] Upon the addition of multivalent salts, the net negative surface charges of the protein molecules are neutralized. Crossing the first critical salt concentration, the solution turns opaque and aggregates, and LLPS or crystallization can be observed. Increasing the salt concentration further yields a charge inversion, and the formally net negatively charged proteins become positive. Upon crossing the second critical salt concentration, the protein salt solution turns clear again, as now the protein molecules repel each other.[4,5,16,25,39,63,65] Thus, a further increase of the salt concentration, exceeding the second critical salt concentration, enhances the net positive surface charge and therefore further enhances the repulsion.[16,39,60,63−65] This experimentally observed behavior corresponds to the physical description of the patchy particle model.[19,66] Previous works by Maier et al.[17,18] reveal that the addition of $CeCl_3$ triggers RC phase behavior for both protein systems. For the tested conditions, only the HSA system exhibited crystallization, whereas BSA did not.

A comparison of the obtained B_2/B_2^{HS} values of BSA and HSA in the presence of 100 mM NaCl and PEG with B_2/B_2^{HS} values for BSA and HSA in the presence of $CeCl_3$ measured by

https://doi.org/10.1021/acs.cgd.4c01535
Cryst. Growth Des. 2025, 25, 2418−2429

Maier et al.[17] reveals that both systems feature similarly low second virial coefficient values (see Figure 6). Since HSA and

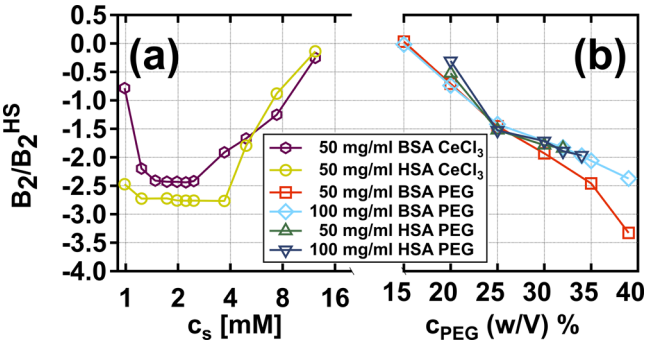

Figure 6. Comparison of (a) B_2/B_2^{HS} values for HSA and BSA in the presence of $CeCl_3$ (data were taken from ref 17) with (b) B_2/B_2^{HS} values of BSA and HSA admixed with PEG. Please note that two separate *X*-axes are provided. The left *X*-axis indicates the $CeCl_3$ concentration (c_s mM) on a logarithmic scale to the base of two (log). The right-hand side *X*-axis indicates the PEG concentration (c_{PEG} (w/V)%) on a linear scale.

BSA exhibit RC phase behavior in the presence of $CeCl_3$, this behavior is also reflected in the virial coefficient analysis. At sufficiently high concentrations of salt (c_{salt}), a steep increase in the B_2/B_2^{HS} values is observed, reflecting the RC behavior (see Figure 6a). Generally, B_2/B_2^{HS} values can be used as a guideline to predict protein crystallization.[52,67] Investigation on protein crystallization showed that virial coefficient values (B_2/B_2^{HS}) within a range of $-10 \lesssim B_2/B_2^{HS} \lesssim -1$ feature a suitable level of attraction between the individual protein molecules for crystallization to occur.[52−54] In addition, ideal growth conditions for crystals were found at two locations in the phase diagram: near but above the critical point or slightly below the critical point. In the first case, density fluctuations are in favor of crystallization, enhancing the nucleation rate, whereas in the second case, the growth of a crystal is facilitated by a two-step process.[67,68]

Interestingly, only HSA crystallized in the presence of $CeCl_3$ provided the investigated conditions despite sufficiently low (attractive) B_2/B_2^{HS} values (see Figure 6a).[17,52−54] The measurements on the BSA− and HSA−PEG systems showed that provided the conditions investigated, only BSA was able to crystallize, again, despite the sufficiently low (attractive) B_2/B_2^{HS} values (see Figure 6b).[52−54]

Moreover, the obtained crystals from the HSA−trivalent salt system (e.g., $CeCl_3$ or YCl_3) exhibit the $P2_12_12_1$ space group.[17,18] The BSA crystals, on the other hand, crystallize in a *C*2 space group. Despite their similarities, small differences require different crystallization strategies, taking into account the experimental conditions used in each study. The X-ray diffraction analysis of BSA crystals and the analysis of the BSA and HSA crystal surfaces is described below.

Discussion on the Different Crystallization Behaviors in the Presence of PEG and Multivalent Salts. The following section addresses both the similarities and differences between BSA and HSA and derives key mechanisms that could trigger the different bulk (crystallization) behaviors of BSA and HSA.

X-ray structure analysis showed that BSA crystals observed in this study are isomorphous to the BSA structure reported by Majorek et al.[40] with unit cell parameters of a = 220.1 Å, b = 44.8 Å, c = 144.4 Å, and β = 114.2° crystallized in space group *C*2. Model coordinates were not further refined, as the crystal packing has already been reported. Next, we compared the crystallographic protein interfaces of BSA and HSA. Both proteins show a sequence identity of 75.6% and adopt a similar protein fold, although their N-terminal domain (residues 1−150 for BSA) differ significantly. The C-terminal amino acids (residues 151−500 for BSA) showed a Cα rmsd of 2.26 Å over 344 aligned residues. It is noteworthy that the combined total mean buried surface area of BSA is substantially lower than that of HSA, with values of 1190 and 1960 Å^2, respectively. However, a reliable statistical analysis is hampered by the limited number of BSA structures deposited with the protein data bank. A randomly picked data set for HSA that we have prepared to avoid user-introduced data bias based on our preselection of reported HSA structures resulted in a comparable total buried surface area of 1890 Å^2 and showed that HSA has in general utilized a larger surface area for crystal contact formation (see Table 1 in the Supporting Information). We mapped all interface areas of the proteins on the surface. Although the pattern of amino acids contributing to crystal contacts looks comparable, HSA utilizes a larger number of residues for crystal contact formation, which indicates a larger number of potential attraction sites for HSA (see Figure 7).

A histogram plot showing the relative frequency of an amino acid to be part of an interface also indicates that HSA utilizes a broader number of residues to take part in protein−protein contact formation (SI Figure 5). A similar conclusion can be made by grouping the interface residues by their number of contacts and plotting their normalized frequency (by the total number of interactions) of the data set (SI Figure 6). This shows that HSA residues possess a wider spread in the number of contacts compared to the BSA data set.

Next, we compared whether BSA is in general capable of establishing a comparable yttrium ion (Y^{3+})-mediated packing, as observed for HSA by building a hypothetical BSA−Y^{3+} lattice similar to pdb entry 7A9C.[18] Both protomers possess a theoretical pI of 5.6 and therefore seem to be capable of forming similar coulombic interactions with positively charged ions. We found that BSA lacks at least one glutamate residue (in BSA A367) that would be essential to form a comparable chelating Y^{3+} complex bridging two HSA protomers, as reported for pdb entry 7A9C.[18] In addition, the formation of salt bridges requires a structural match (recognition) between two protein surfaces and therefore exhibits a strong orientation dependence.[69] This does not, however, exclude a potential complex formation with yttrium ions at a discrete position of a negatively charged patch on the BSA surface.

CONCLUSIONS

In this work, the behavior of the two proteins BSA and HSA in the presence of the polymer PEG M_w 3350 and 100 mM NaCl was investigated. For both protein−PEG systems (BSA and HSA), phase diagrams were established. Both systems featured rich and diverse phase behavior (see Figure 1). However, provided the applied experimental conditions, only the BSA−PEG−salt system featured crystallization, whereas the HSA−PEG−salt system did not. The space group of the BSA crystals was determined by X-ray diffraction analysis. The results confirmed that the space group found corresponds to the previously published *C*2 space group of BSA.[23,40] Based on the ratio of the polymer to colloid size q, it was determined that

https://doi.org/10.1021/acs.cgd.4c01535
Cryst. Growth Des. 2025, 25, 2418−2429

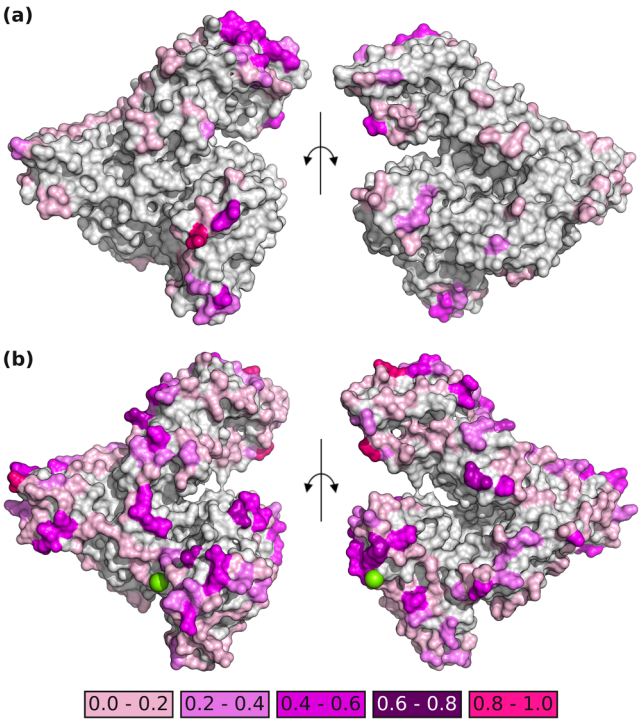

Figure 7. Crystal contact areas of (a) BSA and (b) HSA. The proteins are shown from both sides in similar orientations. The front view is shown on the left, and the back view is shown on the right of each panel (180°). Green spheres indicate the positions of Y^{3+} ions in PDB entry 7A9C. Amino acids involved in crystal contact formation are colored in different shades of violet to pink based on their individual relative weighted surface area from minor impact (light violet) to crucial residues (hot pink). The weighted surface area is calculated by the summation of all crystal contact area contributions of an individual residue over interfaces in all pdb entries of the chosen data set. A cutoff value of 20 Å^2 is applied, and residues below this cutoff value are neglected from the calculation. A detailed analysis that takes different cutoff values into account is presented in the Supporting Information (SI Figures 3 and 4). The individual summed per residue surface area is then divided by the largest individual per residue surface area to obtain an individual (per residue) relative weighted surface area that is not dependent on the number of all investigated contact interfaces.

the colloid limit $q < 1$ applies. This calculated size ratio allows the experimental phase behavior to be compared with those obtained from colloid−polymer theory within the framework of depletion interactions. Results revealed an agreement between the theoretical and experimental phase diagrams,[70] suggesting that the phase behavior can be attributed to simple depletion interactions. Furthermore, it cannot be ruled out that apart from the depletion effect, other interactions or effects interfere and trigger the observed phase behavior. These could include hydration effects, hydrophobic interactions, or even dispersion forces. However, the protein−polymer solutions do not form aggregates in the following three cases: absence of the polymer (PEG M_w 3350) and salt (100 mM NaCl), presence of salt and absence of the polymer,[71−73] and presence of the polymer and absence of salt.[74] This suggests that the observed phase behavior can be attributed to depletion interaction. In order to maintain this reasoning, it is necessary to consider the structure of the colloids from a coarse-grained perspective, which allows us to describe the proteins as hard spheres. Given the absence of salt and polymers, BSA and HSA solutions are stable up to high concentrations, which indicates only minor interactions.

In addition to the phase behavior, SAXS measurements were conducted in order to further quantify the protein−PEG−salt systems by means of a second virial coefficient analysis (B_2/B_2^{HS}). It was shown that with increasing PEG concentration, B_2/B_2^{HS} decreases; thus, both systems increase their attractiveness. Additionally, both systems feature B_2/B_2^{HS} values corresponding to $-10 \lesssim B_2/B_2^{HS} \lesssim -1$.[52−54] This clearly indicates that both protein−polymer−salt systems feature low enough B_2/B_2^{HS} values for crystallization. However, as mentioned above, crystallization was observed only for the BSA−PEG−salt system. Moreover, the obtained B_2/B_2^{HS} values were compared to B_2/B_2^{HS} for BSA− and HSA−$CeCl_3$−salt systems recorded by Maier et al.[17] (see Figure 6). Interestingly, for BSA and HSA with $CeCl_3$, similarly low B_2/B_2^{HS} values were recorded, indicating that both BSA and HSA could potentially form crystals. However, utilizing $CeCl_3$, only the HSA system showed crystallization.

Next, a crystal surface analysis of HSA and BSA revealed that HSA utilizes a greater number of solvent-exposed amino acids for intermolecular protein−protein interactions, eventually resulting in crystal formation. This agrees with the large number of reported crystal structures in the protein database, where 118 HSA entries are reported to form at least 13 different crystal packings. In contrast, eight BSA entries are found in the protein data bank, all crystallized in an isomorphous crystal packing of space group *C*2. Although the sequence similarity of approximately 76% and a comparable isoelectric point of 5.6 for both proteins suggest a closely related phase behavior, their crystallization properties are fundamentally different. This is further demonstrated by their different behavior with respect to Y^{3+} ions. Although HSA is capable of forming cation-mediated intermolecular protein−protein interfaces via positively charged Y^{3+} ions, a comparable behavior is not observed for BSA, as the crucial acidic residues are either not found at the HSA-specific positions or adopt conformation that would not allow for a comparable chelating effect. This clearly indicates that the phase behavior of a protein is not directly accessible by the phase diagram of closely related proteins, as minor changes in the surface landscape render it necessary to determine the phase diagram for every protein candidate individually.

EXPERIMENTAL SECTION

Materials and Sample Preparation. Proteins BSA (A3733, purity of ≤98%) and HSA (A9511, purity of ≤97%), sodium azide (NaN_3) (S8032-25G), and poly(ethylene glycol) powder (PEG, $H(OCH_2CH_2)nOH$, average size of M_w 3350, 202444-250G) were purchased from Sigma-Aldrich, now Merck, and used in the executed experiments without further purification. Similarly, sodium chloride (NaCl) was purchased from Merck and, without further purification, used in the experiments. In order to prevent any contamination caused by unwanted bacterial or fungal growth, 1 mM NaN_3 was added to deionized and degassed Millipore water (a conductivity of 18.2 MΩ cm). This Millipore water was then used to prepare stock solutions by dissolving the required amounts of protein powder, NaCl, or PEG. The stock solutions were prepared at room temperature (RT, 21 ± 1 °C).

After preparation, the protein stock solutions were immediately incubated for at least 24 h at 4 °C to ensure the dissolution of protein powder. The concentration of the protein stock solution was determined by a Cray 50 UV−vis spectrophotometer (Varian Technologies) with appropriate extinction coefficients (see Table 1) and Cary WinUV operating software. The absorbance was measured

https://doi.org/10.1021/acs.cgd.4c01535
Cryst. Growth Des. 2025, 25, 2418−2429

at 280 nm. The protein solutions were stored at 4 °C in air-impermeable containers to avoid the redissolution of gases.[75] Moreover, the protein solutions were used exclusively for a total duration of 3 weeks.[76] The PEG stock solution was prepared using a weight-to-volume ratio (w/V)% of 100% (1 g of PEG to 1 mL of Millipore water). The PEG solution and the salt solution were stored at RT. All samples were obtained by mixing the required amount of the previously prepared Millipore water, protein stock solution, PEG stock solution, and NaCl stock solution. The prepared samples showed a pH value well above the pI of the respective protein, measured with a pH meter from Mettler Toledo (Germany). Investigation of the samples was carried out at RT. Systematic deviations arising from variations in protein batches, preparative inaccuracies, and fluctuations in protein and other stock solutions cannot be ruled out.

BSA and HSA Phase Behavior Determination. Visual inspection was performed to determine the phase diagrams for BSA and HSA (Figure 1) in the presence of PEG and NaCl. According to this, a sample series with four different protein concentrations (20, 50, 80, and 100 mg/mL) accompanied by 100 mM NaCl and increasing PEG concentrations (w/V)% were prepared for BSA and HSA, respectively. To avoid confusion, t^* is defined as the transition border from a clear sample to a turbid one, as seen in Figure 1.

Besides inspection by the eye, an optical microscope (Axio Scope.A1, Carl Zeiss AG) was used for a more precise optical investigation of the samples. Images were recorded by a camera (AxioCam ICc5, Carl Zeiss AG) operated with software ZEN Lite 2012. Microscopy samples were collected from the respective previously prepared phase diagram sample series. This involved dispensing 25 μL of sample onto a Gene Frame (1 cm × 1 cm) with a thickness of 0.25 mm (Thermo Scientific, Germany). Afterward, the Gene Frame was covered with a coverslip. In order to investigate crystallization, appropriate samples (in tubes or microscopy slides) were stored and observed over a longer period of time ranging from 7 days (microscopy slides) to 1 month (tubes).

SAXS and Data Analysis. In small-angle X-ray scattering (SAXS) experiments dealing with suspended particles in solution, the measured intensity profile $I(Q)$ can be described as a function of the momentum transfer Q

$$I(Q) \propto n_p \Delta\rho^2 V_p^2 \langle P(Q)\rangle S(Q) \tag{6}$$

This relation is given for monodisperse and spherical particles. The number density of the dissolved particles is given by n_p, while $\Delta\rho$ denotes the cross-sectional scattering difference between the particle and the solvent. V_p represents the volume of the particle. The momentum transfer is defined as $Q = (4\pi/\lambda)\sin(2\theta/2)$. Here, λ denotes the wavelength and 2θ denotes the scattering angle. The shape and size of the scattered particle averaged over the spatial orientation are given by form factor $\langle P(Q)\rangle$. $S(Q)$ denotes the structural factor, describing the spatial arrangement of the particles, which is governed by the interaction potential. From this, it can be deduced that the structural factor $S(Q)$ describes the effect of positional correlations.[55,84]

SAXS data was collected at the P12 beamline of EMBL (DESY, Hamburg, Germany). The measurement setup used utilizes a focused X-ray beam (120 μm × 200 μm) with an energy of 10 keV and a corresponding wavelength of λ = 1.24 Å. The sample-to-detector distance was set to 3.1 m. A Q range of 0.002−0.45 Å^{-1} was covered by a 2 M Pilatus (Dectris) detector. Prior to the measurement, the samples were carefully centrifuged, and subsequently, the supernatant was measured. Each sample was illuminated for 30 exposures, with a duration of 0.095 s each. Exchanging of samples was realized by a flow cell. The intensity profiles were obtained by azimuthal averaging of the collected 2D data sets. Averaging of each data set was performed only after a manual check for consistency. Inconsistent exposures due to, e.g., air bubbles in the flow cell were sorted out. Unlike its behavior in neutron scattering experiments, PEG has an almost identical X-ray scattering cross section per unit volume to H_2O, allowing the polymer salt mixture to be considered background.[85] The background measurements were treated likewise and then subtracted from the sample profiles. By subtraction of the defined background, SAXS scattering curves (Figure 4) were obtained, containing solely the contribution from the proteins. The averaged background measurements used for subtraction are given in the Supporting Information (SI Figure 2).

Data analysis was performed using an IGOR PRO 9 add-on provided by the National Institute of Standards and Technology (NIST).[86] The background-corrected data sets were fitted using the sticky hard-sphere potential (SHS),[87] utilizing an ellipsoidal form factor. A similar pipeline for SAXS data processing can be found in refs 59,88,89. The SHS potential for a spherical particle of radius R is defined in eq 7.

$$\beta U(r) = \begin{cases} \infty & r < \sigma = 2R \\ -\beta_0 = \ln\left(\dfrac{12\tau\Delta}{\sigma + \Delta}\right) & r < \sigma = 2R \\ 0 & r > \sigma + \Delta \end{cases} \tag{7}$$

Here, β indicates the inverse of the thermal energy, $1/k_BT$. τ indicates the stickiness parameter, Δ indicates the width of the square well, and σ indicates the diameter of the hard sphere. Based on the perturbative solution of the Percus−Yevick closure relation, the structure factor was calculated.[87,90] Equation 8 shows the calculation for the reduced second virial coefficient within the limitation of $\Delta \to 0$.

$$\lim_{\Delta\to 0} \frac{B_2}{B_2^{HS}} = 1 - \frac{1}{4\tau} \tag{8}$$

To obtain the reduced second virial coefficient, we divided the second virial coefficient (B_2) with the second virial coefficient for hard spheres (B_2^{HS}) of radius R. This relation is given by $B_2^{HS} = 16\pi R^3/3$. Combining the results from simulations and theories has led to a universal B_2/B_2^{HS} value of ≈ −1.5 for the liquid−gas transition in a multitude of different systems, provided that the Percus−Yevick closure relation is applied.[58,67]

The protein concentration within the supernatant (dilute phase) was determined by averaging ten intensity values at high $Q \approx 0.4$ Å^{-1} of a nonphase-separated (control) sample at 50 and 100 mg/mL. Similarly, these intensity values were taken from each sample individually. The protein concentration was calculated by dividing the intensity value of the nonphase-separated respective control by the intensity value of the sample, followed by multiplying the result by 100. The protein concentration (mg/mL) values thus obtained were then used to calculate the protein volume fraction. This correction was necessary because only the supernatant was measurable due to phase separation and aggregation, thus ensuring comparability.

Besides the volume fraction, the axes of the ellipsoids were fixed to the values shown in Table 1. Moreover, the scattering length density (SLD) of the proteins was set to 7.32 × 10^{-7} Å^{-2}. The background was set to appropriate values for each curve individually. In order to prevent artificial coupling between the well width Δ and stickiness parameter τ, Δ was kept at 0.01σ for all fitted data.

BSA Crystal Analysis and Packing Comparison of HSA with BSA. BSA crystals were analyzed by single-crystal X-ray diffraction experiments. Therefore, single crystals of the suspension were extracted. To cryoprotect the crystals, the supernatant of the suspension was supplemented with glycerol (26 w/V %). BSA crystals were transferred in the cryo solution, rapidly washed, mounted into a loop, and flash-frozen in liquid nitrogen before data collection at beamline X06SA (swiss light source, Villigen, Switzerland). Although several crystals were tested, the diffraction quality remained limited, with the best diffracting crystals yielding a high resolution of approximately 3.5 Å. This was sufficient to unequivocally determine the crystal packing using XDS.[91] The protein crystallized in space group $C2$ with unit cell parameters of a = 220.1 Å, b = 44.8 Å, c = 144.4 Å, and β = 114.2°. A comparison of all BSA structures deposited to the protein data bank revealed a similar crystal packing with cell parameters of a = 215.66 Å, b = 45.10 Å, c = 142.41 Å, and β = 114.0°, as reported by Majorek et al.,[40] and therefore yield to the

https://doi.org/10.1021/acs.cgd.4c01535
Cryst. Growth Des. 2025, 25, 2418−2429

decision to not further refine the resulting structure but to focus on a detailed interface analysis of available BSA and HSA structures. As a consequence, we searched the protein data bank for structures of human serum albumin and bovine serum albumin, yielding 113 entries for HSA and eight entries for BSA. For BSA, all annotated structures resulted from isomorphous crystal packing of space group C2 with unit cell parameters very close to a = 215.7 Å, b = 45.1 Å, c = 142.4 Å, and β = 114.0°. Our packing analysis of HSA excluded all structures where HSA was determined by either Cryo-EM or NMR and those in which HSA was complexed with a proteinogenic interaction partner, resulting in a data set of 97 HSA structures. Next, we sorted these entries by the reported crystallographic space group and assessed their isomorphism based on the unit cell parameters, yielding a data set separated into 14 groups. Out of this data set, we picked ten structures that used either PEG molecules or phosphate/salt conditions for the crystallization experiment and analyzed the crystal packing interfaces using EPPIC.[92] As the selection is user-biased, we decided to include a second analysis utilizing the same data set but randomly picked ten structures, chosing a single member per group from the 14 groups and avoiding duplicate entries. For further analysis, we annotated the size of each crystallographic interface, the amino acids contributing to a crystallographic interface, and the frequency of each amino acid's contribution to packing. In addition, we performed a surface area-based analysis, investigating the individual contribution of a residue to a crystallographic contact by calculating its surface area using PDBePISA.[93] Moreover, we performed the same analysis based on the frequency with which a residue was found in an interface. We performed the same analysis for all data sets, including the data set chosen based on the crystallization conditions and the randomized data set, and compared the data to the available data for BSA. We generated surface representations of BSA and HSA using PYMOL (The PyMOL Molecular Graphics System, version 3.0, Schrödinger, LLC) and colored the amino acids contributing to interface formation based on how often these residues are reported in an interface area (see Figure 7).

■ ASSOCIATED CONTENT

Data Availability Statement

Data are available free of charge upon reasonable request.

Supporting Information

The Supporting Information is available free of charge at https://pubs.acs.org/doi/10.1021/acs.cgd.4c01535.

Images of samples used for visual inspection of BSA and HSA; Scattering backgrounds for 100 mM NaCl with increasing concentrations of PEG; Interface analysis of HSA and BSA structures; Crystal contact analysis of BSA and HSA, histogram plots and interface residues grouped by the number of their contacts within all interfaces (PDF)

■ AUTHOR INFORMATION

Corresponding Authors

Maximilian D. Senft − *Institut für Angewandte Physik, Universität Tübingen, 72076 Tübingen, Germany;* orcid.org/0000-0002-0646-7918; Email: Maximilian.Senft@uni-tuebingen.de

Georg Zocher − *Interfakultäres Institut für Biochemie (IFIB), Universität Tübingen, 72076 Tübingen, Germany;* orcid.org/0000-0001-8711-2088; Email: Georg.Zocher@uni-tuebingen.de

Fajun Zhang − *Institut für Angewandte Physik, Universität Tübingen, 72076 Tübingen, Germany;* orcid.org/0000-0001-7639-8594; Email: Fajun.Zhang@uni-tuebingen.de

Authors

Sebastian Retzbach − *Institut für Angewandte Physik, Universität Tübingen, 72076 Tübingen, Germany;* orcid.org/0000-0001-5908-7823

Ralph Maier − *Institut für Angewandte Physik, Universität Tübingen, 72076 Tübingen, Germany;* orcid.org/0000-0003-3428-039X

Anusha Hiremath − *Institut für Angewandte Physik, Universität Tübingen, 72076 Tübingen, Germany*

Thilo Stehle − *Interfakultäres Institut für Biochemie (IFIB), Universität Tübingen, 72076 Tübingen, Germany;* orcid.org/0000-0002-4571-8548

Frank Schreiber − *Institut für Angewandte Physik, Universität Tübingen, 72076 Tübingen, Germany;* orcid.org/0000-0003-3659-6718

Complete contact information is available at: https://pubs.acs.org/10.1021/acs.cgd.4c01535

Notes

The authors declare no competing financial interest.

■ ACKNOWLEDGMENTS

The authors gratefully acknowledge financial support from the DFG and BMBF, as well as the allocation of beamtime and the support of the beamline scientists at P12 (PETRA III, Hamburg, Germany). The authors appreciate the fruitful discussions with Dr. Stefano DaVela, Dr. Dmitry Lapkin, and Dr. Ivan Zaluzhnyy. The authors thank Umar-Abdullahi Janyau, Marcell Bäcker, and Jeronimo Dey for experimental assistance.

■ REFERENCES

(1) McPherson, A.; Gavira, J. A. Introduction to protein crystallization. *Acta Crystallogr., Sect. F: Struct. Biol. Commun.* **2014**, *70*, 2−20.

(2) Asherie, N. Protein crystallization and phase diagrams. *Methods* **2004**, *34*, 266−272.

(3) McPherson, A. *Crystallization of Biological Micromolecules*; Cold Spring Harbor Laboratory Press: New York, NY, 1998.

(4) Zhang, F.; Roth, R.; Wolf, M.; Roosen-Runge, F.; Skoda, M. W.; Jacobs, R. M.; Stzucki, M.; Schreiber, F. Charge-controlled metastable liquid−liquid phase separation in protein solutions as a universal pathway towards crystallization. *Soft Matter* **2012**, *8*, 1313−1316.

(5) Zhang, F. Nonclassical nucleation pathways in protein crystallization. *J. Phys.: Condens. Matter* **2017**, *29*, No. 443002.

(6) Alberti, S.; Gladfelter, A.; Mittag, T. Considerations and challenges in studying liquid-liquid phase separation and biomolecular condensates. *Cell* **2019**, *176*, 419−434.

(7) Kakio, A.; Nishimoto, S.-i.; Yanagisawa, K.; Kozutsumi, Y.; Matsuzaki, K. Cholesterol-dependent formation of GM1 ganglioside-bound amyloid β-protein, an endogenous seed for Alzheimer amyloid. *J. Biol. Chem.* **2001**, *276*, 24985−24990.

(8) Cohen, S. I. A.; Linse, S.; Luheshi, L. M.; Hellstrand, E.; White, D. A.; Rajah, L.; Otzen, D. E.; Vendruscolo, M.; Dobson, C. M.; Knowles, T. P. Proliferation of amyloid-β42 aggregates occurs through a secondary nucleation mechanism. *Proc. Natl. Acad. Sci. U.S.A.* **2013**, *110*, 9758−9763.

(9) Larson, A. G.; Elnatan, D.; Keenen, M. M.; Trnka, M. J.; Johnston, J. B.; Burlingame, A. L.; Agard, D. A.; Redding, S.; Narlikar, G. J. Liquid droplet formation by HP1α suggests a role for phase separation in heterochromatin. *Nature* **2017**, *547*, 236−240.

(10) Kilic, S.; Lezaja, A.; Gatti, M.; Bianco, E.; Michelena, J.; Imhof, R.; Altmeyer, M. Phase separation of 53 BP 1 determines liquid-like behavior of DNA repair compartments. *EMBO J.* **2019**, *38*, No. e101379.

(11) Acharya, K. R.; Ackerman, S. J. Eosinophil granule proteins: form and function. *J. Biol. Chem.* **2014**, *289*, 17406−17415.
(12) Liu, C.; Yan, B.; Qi, S.; Zhang, Y.; Zhang, L.; Wang, C. Predictive significance of Charcot−Leyden crystals for eosinophilic chronic rhinosinusitis with nasal polyps. *Am. J. Rhinol. Allergy* **2019**, *33*, 671−680.
(13) Weller, P. F. Eosinophilia. *J. Allergy Clin. Immunol.* **1984**, *73*, 1−10.
(14) Davis, B. P.; Rothenberg, M. E. Eosinophils and cancer. *Cancer Immunol. Res.* **2014**, *2*, 1−8.
(15) Pande, A.; Pande, J.; Asherie, N.; Lomakin, A.; Ogun, O.; King, J.; Benedek, G. B. Crystal cataracts: human genetic cataract caused by protein crystallization. *Proc. Natl. Acad. Sci. U.S.A.* **2001**, *98*, 6116−6120.
(16) Zhang, F.; Zocher, G.; Sauter, A.; Stehle, T.; Schreiber, F. Novel approach to controlled protein crystallization through ligandation of yttrium cations. *J. Appl. Crystallogr.* **2011**, *44*, 755−762.
(17) Maier, R.; Fries, M. R.; Buchholz, C.; Zhang, F.; Schreiber, F. Human versus bovine serum albumin: a subtle difference in hydrophobicity leads to large differences in bulk and interface behavior. *Cryst. Growth Des.* **2021**, *21*, 5451−5459.
(18) Maier, R.; Zocher, G.; Sauter, A.; Da Vela, S.; Matsarskaia, O.; Schweins, R.; Sztucki, M.; Zhang, F.; Stehle, T.; Schreiber, F. Protein crystallization in the presence of a metastable liquid−liquid phase separation. *Cryst. Growth Des.* **2020**, *20*, 7951−7962.
(19) Roosen-Runge, F.; Zhang, F.; Schreiber, F.; Roth, R. Ion-activated attractive patches as a mechanism for controlled protein interactions. *Sci. Rep.* **2014**, *4*, No. 7016.
(20) Peters, T., Jr *All About Albumin: Biochemistry, Genetics, and Medical Applications*; Academic Press, 1995.
(21) Barbosa, L. R.; Ortore, M. G.; Spinozzi, F.; Mariani, P.; Bernstorff, S.; Itri, R. The importance of protein-protein interactions on the pH-induced conformational changes of bovine serum albumin: a small-angle X-ray scattering study. *Biophys. J.* **2010**, *98*, 147−157.
(22) Sugio, S.; Kashima, A.; Mochizuki, S.; Noda, M.; Kobayashi, K. Crystal structure of human serum albumin at 2.5 Å resolution. *Protein Eng.* **1999**, *12*, 439−446.
(23) Bujacz, A. Structures of bovine, equine and leporine serum albumin. *Acta Crystallogr., Sect. D: Biol. Crystallogr.* **2012**, *68*, 1278−1289.
(24) Bujacz, A.; Zielinski, K.; Sekula, B. Structural studies of bovine, equine, and leporine serum albumin complexes with naproxen. *Proteins: Struct., Funct., Bioinf.* **2014**, *82*, 2199−2208.
(25) Zhang, F.; Weggler, S.; Ziller, M. J.; Ianeselli, L.; Heck, B. S.; Hildebrandt, A.; Kohlbacher, O.; Skoda, M. W.; Jacobs, R. M.; Schreiber, F. Universality of protein reentrant condensation in solution induced by multivalent metal ions. *Proteins: Struct., Funct., Bioinf.* **2010**, *78*, 3450−3457.
(26) Hunter, R. *Foundations of Colloid Science*; Oxford University Press, 2001.
(27) Lekkerkerker, H. N.; Tuinier, R.*Colloids and the Depletion Interaction*; Springer, 2011; pp 57−108.
(28) Asakura, S.; Oosawa, F. On interaction between two bodies immersed in a solution of macromolecules. *J. Chem. Phys.* **1954**, *22*, 1255−1256.
(29) Asakura, S.; Oosawa, F. Interaction between particles suspended in solutions of macromolecules. *J. Polym. Sci.* **1958**, *33*, 183−192.
(30) Vrij, A. Polymers at interfaces and the interactions in colloidal dispersions. *Pure Appl. Chem.* **1976**, *48*, 471−483.
(31) Mutch, K. J.; van Duijneveldt, J. S.; Eastoe, J.; Grillo, I.; Heenan, R. K. Small-angle neutron scattering study of microemulsion-polymer mixtures in the protein limit. *Langmuir* **2008**, *24*, 3053−3060.
(32) Mutch, K. J.; van Duijneveldt, J. S.; Eastoe, J. Colloid−polymer mixtures in the protein limit. *Soft Matter* **2007**, *3*, 155−167.
(33) Bolhuis, P. G.; Meijer, E. J.; Louis, A. A. Colloid-polymer mixtures in the protein limit. *Phys. Rev. Lett.* **2003**, *90*, No. 068304.
(34) Arakawa, T.; Timasheff, S. N. Mechanism of polyethylene glycol interaction with proteins. *Biochemistry* **1985**, *24*, 6756−6762.
(35) Israelachvili, J. The different faces of poly (ethylene glycol). *Proc. Natl. Acad. Sci. U.S.A.* **1997**, *94*, 8378−8379.
(36) Harris, J. M. *Poly(Ethylene Glycol)Chemistry: Biotechnical and Biomedical Applications*; Springer Science & Business Media, 1992.
(37) Maxfield, J.; Shepherd, I. Conformation of poly (ethylene oxide) in the solid state, melt and solution measured by Raman scattering. *Polymer* **1975**, *16*, 505−509.
(38) Chanphai, P.; Bekale, L.; Sanyakamdhorn, S.; Agudelo, D.; Tajmir-Riahi, H.-A. Effect of synthetic polymers on polymer−protein interaction. *Polymer* **2014**, *55*, 572−582.
(39) Zhang, F.; Skoda, M. W. A.; Jacobs, R. M. J.; Zorn, S.; Martin, R. A.; Martin, C. M.; Clark, G. F.; Weggler, S.; Hildebrandt, A.; Kohlbacher, O.; Schreiber, F. Reentrant condensation of proteins in solution induced by multivalent counterions. *Phys. Rev. Lett.* **2008**, *101*, No. 148101.
(40) Majorek, K. A.; Porebski, P. J.; Dayal, A.; Zimmerman, M. D.; Jablonska, K.; Stewart, A. J.; Chruszcz, M.; Minor, W. Structural and immunologic characterization of bovine, horse, and rabbit serum albumins. *Mol. Immunol.* **2012**, *52*, 174−182.
(41) Zunszain, P. A.; Ghuman, J.; Komatsu, T.; Tsuchida, E.; Curry, S. Crystal structural analysis of human serum albumin complexed with hemin and fatty acid. *BMC Struct. Biol.* **2003**, *3*, No. 6.
(42) Devanand, K.; Selser, J. Asymptotic behavior and long-range interactions in aqueous solutions of poly (ethylene oxide). *Macromolecules* **1991**, *24*, 5943−5947.
(43) Gurnev, P. A.; Stanley, C. B.; Aksoyoglu, M. A.; Hong, K.; Parsegian, V. A.; Bezrukov, S. M. Poly(ethylene glycol)s in Semidilute Regime: Radius of Gyration in the Bulk and Partitioning into a Nanopore. *Macromolecules* **2017**, *50*, 2477−2483.
(44) Teraoka, I. *Polymer Solutions: An Introduction to Physical Properties*; Wiley & Sons. Inc. Publication: New York, 2002.
(45) De Gennes, P.-G. *Scaling Concepts in Polymer Physics*; Cornell University Press, 1979.
(46) Mao, Y.; Cates, M.; Lekkerkerker, H. Depletion force in colloidal systems. *Phys. A* **1995**, *222*, 10−24.
(47) Vivarès, D.; Belloni, L.; Tardieu, A.; Bonneté, F. Catching the PEG-induced attractive interaction between proteins. *Eur. Phys. J. E* **2002**, *9*, 15−25.
(48) Poon, W.; Pusey, P.; Lekkerkerker, H. Colloids in suspense. *Phys. World* **1996**, *9*, No. 27.
(49) Poon, W. C. K.; Selfe, J. S.; Robertson, M. B.; Ilett, S. M.; Pirie, A. D.; Pusey, P. N. An experimental study of a model colloid-polymer mixture. *J. Phys. II* **1993**, *3*, 1075−1086.
(50) Calderon, F. L.; Bibette, J.; Biais, J. Experimental phase diagrams of polymer and colloid mixtures. *Europhys. Lett. (EPL)* **1993**, *23*, 653−659.
(51) Lekkerkerker, H. N. W.; Poon, W. C.-K.; Pusey, P. N.; Stroobants, A.; Warren, P. B. Phase behaviour of Colloid + polymer mixtures. *Europhys. Lett. (EPL)* **1992**, *20*, 559−564.
(52) George, A.; Wilson, W. W. Predicting protein crystallization from a dilute solution property. *Acta Crystallogr., Sect. D: Biol. Crystallogr.* **1994**, *50*, 361−365.
(53) Platten, F.; Hansen, J.; Wagner, D.; Egelhaaf, S. U. Second virial coefficient as determined from protein phase behavior. *J. Phys. Chem. Lett.* **2016**, *7*, 4008−4014.
(54) Hentschel, L.; Hansen, J.; Egelhaaf, S. U.; Platten, F. The crystallization enthalpy and entropy of protein solutions: microcalorimetry, van't Hoff determination and linearized Poisson−Boltzmann model of tetragonal lysozyme crystals. *Phys. Chem. Chem. Phys.* **2021**, *23*, 2686−2696.
(55) Linder, P.; Zemb, T. *Neutrons, X-rays, and Light: Scattering Methods Applied to Soft Condensed Matter*, 1st ed.; Delta Series-Elsevier, 2002.
(56) Hansen, J.-P.; McDonald, I. R. *Theory of Simple Liquids: with Applications to Soft Matter*, 3rd ed.; Academic Press, Elsevier, 2006.

https://doi.org/10.1021/acs.cgd.4c01535
Cryst. Growth Des. 2025, 25, 2418−2429

(57) Gunton, J. D.; Shiryayev, A.; Pagan, D. L. *Protein Condensation: Kinetic Pathways to Crystallization and Disease*, 1st ed.; Cambridge University Press, 2014.
(58) Noro, M. G.; Frenkel, D. Extended corresponding-states behavior for particles with variable range attractions. *J. Chem. Phys.* **2000**, *113*, 2941−2944.
(59) Braun, M. K.; Sauter, A.; Matsarskaia, O.; Wolf, M.; Roosen-Runge, F.; Sztucki, M.; Roth, R.; Zhang, F.; Schreiber, F. Reentrant phase behavior in protein solutions induced by multivalent salts: strong effect of anions Cl−versus NO3−. *J. Phys. Chem. B* **2018**, *122*, 11978−11985.
(60) Matsarskaia, O.; Braun, M. K.; Roosen-Runge, F.; Wolf, M.; Zhang, F.; Roth, R.; Schreiber, F. Cation-induced hydration effects cause lower critical solution temperature behavior in protein solutions. *J. Phys. Chem. B* **2016**, *120*, 7731−7736.
(61) Matsarskaia, O.; Roosen-Runge, F.; Schreiber, F. Multivalent ions and biomolecules: Attempting a comprehensive perspective. *ChemPhysChem* **2020**, *21*, 1742−1767.
(62) Zhang, F.; Roosen-Runge, F.; Sauter, A.; Wolf, M.; Jacobs, R. M.; Schreiber, F. Reentrant condensation, liquid−liquid phase separation and crystallization in protein solutions induced by multivalent metal ions. *Pure Appl. Chem.* **2014**, *86*, 191−202.
(63) Soraruf, D.; Roosen-Runge, F.; Grimaldo, M.; Zanini, F.; Schweins, R.; Seydel, T.; Zhang, F.; Roth, R.; Oettel, M.; Schreiber, F. Protein cluster formation in aqueous solution in the presence of multivalent metal ions−a light scattering study. *Soft Matter* **2014**, *10*, 894−902.
(64) Roosen-Runge, F.; Heck, B. S.; Zhang, F.; Kohlbacher, O.; Schreiber, F. Interplay of pH and binding of multivalent metal ions: charge inversion and reentrant condensation in protein solutions. *J. Phys. Chem. B* **2013**, *117*, 5777−5787.
(65) Zhang, F.; Roosen-Runge, F.; Sauter, A.; Roth, R.; Skoda, M. W. A.; Jacobs, R. M. J.; Sztucki, M.; Schreiber, F. The role of cluster formation and metastable liquid−liquid phase separation in protein crystallization. *Faraday Discuss.* **2012**, *159*, 313−325.
(66) Surfaro, F.; Zhang, F.; Schreiber, F.; Roth, R. The ion-activated attractive patchy particle model and its application to the liquid−vapor phase transitions. *J. Chem. Phys.* **2024**, *161*, No. 034901, DOI: 10.1063/5.0215920.
(67) Vliegenthart, G. A.; Lekkerkerker, H. N. Predicting the gas−liquid critical point from the second virial coefficient. *J. Chem. Phys.* **2000**, *112*, 5364−5369.
(68) ten Wolde, P. R.; Frenkel, D. Enhancement of protein crystal nucleation by critical density fluctuations. *Science* **1997**, *277*, 1975−1978.
(69) Fusco, D.; Charbonneau, P. Soft matter perspective on protein crystal assembly. *Colloids Surf., B* **2016**, *137*, 22−31.
(70) Anderson, V. J.; Lekkerkerker, H. N. Insights into phase transition kinetics from colloid science. *Nature* **2002**, *416*, 811−815.
(71) Zhang, F.; Skoda, M. W.; Jacobs, R. M.; Martin, R. A.; Martin, C. M.; Schreiber, F. Protein interactions studied by SAXS: effect of ionic strength and protein concentration for BSA in aqueous solutions. *J. Phys. Chem. B* **2007**, *111*, 251−259.
(72) Zhang, F.; Roosen-Runge, F.; Skoda, M. W.; Jacobs, R. M.; Wolf, M.; Callow, P.; Frielinghaus, H.; Pipich, V.; Prevost, S.; Schreiber, F. Hydration and interactions in protein solutions containing concentrated electrolytes studied by small-angle scattering. *Phys. Chem. Chem. Phys.* **2012**, *14*, 2483−2493.
(73) Pellicane, G.; Cavero, M. Theoretical study of interactions of BSA protein in a NaCl aqueous solution. *J. Chem. Phys.* **2013**, *138*, No. 115103, DOI: 10.1063/1.4794919.
(74) Lai, J.-j.; Yan, H.-y.; Liu, Y.; Huang, Y. Effects of PEG molecular weight on its interaction with albumin. *Chin. J. Polym. Sci.* **2015**, *33*, 1373−1379.
(75) Zhang, X. H.; Zhang, X. D.; Lou, S. T.; Zhang, Z. X.; Sun, J. L.; Hu, J.; et al. Degassing and temperature effects on the formation of nanobubbles at the mica/water interface. *Langmuir* **2004**, *20*, 3813−3815.
(76) Mirtallo, J. M.; Caryer, K.; Schneider, P. J.; Ayers, L.; Fabri, P. J. Growth of bacteria and fungi in parenteral nutrition solutions containing albumin. *Am. J. Hosp. Pharm.* **1981**, *38*, 1907−1910.
(77) Yang, M.; Dutta, C.; Tiwari, A. Disulfide-bond scrambling promotes amorphous aggregates in lysozyme and bovine serum albumin. *J. Phys. Chem. B* **2015**, *119*, 3969−3981.
(78) Hirayama, K.; Akashi, S.; Furuya, M.; Fukuhara, K.-i. Rapid confirmation and revision of the primary structure of bovine serum albumin by ESIMS and Frit-FAB LC/MS. *Biochem. Biophys. Res. Commun.* **1990**, *173*, 639−646.
(79) Jachimska, B.; Wasilewska, M.; Adamczyk, Z. Characterization of globular protein solutions by dynamic light scattering, electrophoretic mobility, and viscosity measurements. *Langmuir* **2008**, *24*, 6866−6872.
(80) Dockal, M.; Carter, D. C.; Ruker, F. Conformational transitions of the three recombinant domains of human serum albumin depending on pH. *J. Biol. Chem.* **2000**, *275*, 3042−3050.
(81) Lee, J. C.; Timasheff, S. N. Partial specific volumes and interactions with solvent components of proteins in guanidine hydrochloride. *Biochemistry* **1974**, *13*, 257−265.
(82) Hianik, T.; Poniková, S.; Bágel'ová, J.; Antalík, M. Specific volume and compressibility of human serum albumin−polyanion complexes. *Bioorg. Med. Chem. Lett.* **2006**, *16*, 274−279.
(83) Lundblad, R. L.; Macdonald, F. *Handbook of Biochemistry and Molecular Biology*; CRC Press, 2018.
(84) Pedersen, J. S. Analysis of small-angle scattering data from colloids and polymer solutions: modeling and least-squares fitting. *Adv. Colloid Interface Sci.* **1997**, *70*, 171−210.
(85) Thiyagarajan, P.; Chaiko, D.; Hjelm, R., Jr A neutron scattering study of poly (ethylene glycol) in electrolyte solutions. *Macromolecules* **1995**, *28*, 7730−7736.
(86) Kline, S. R. Reduction and analysis of SANS and USANS data using IGOR Pro. *J. Appl. Crystallogr.* **2006**, *39*, 895−900.
(87) Baxter, R. J. Percus−Yevick equation for hard spheres with surface adhesion. *J. Chem. Phys.* **1968**, *49*, 2770−2774.
(88) Braun, M. K.; Wolf, M.; Matsarskaia, O.; Da Vela, S.; Roosen-Runge, F.; Sztucki, M.; Roth, R.; Zhang, F.; Schreiber, F. Strong Isotope Effects on Effective Interactions and Phase Behavior in Protein Solutions in the Presence of Multivalent Ions. *J. Phys. Chem. B* **2017**, *121*, 1731−1739.
(89) Senft, M. D.; Maier, R.; Hiremath, A.; Zhang, F.; Schreiber, F. Effective interactions and phase behavior of protein solutions in the presence of hexamine cobalt(III) chloride. *Eur. Phys. J. E* **2023**, *46*, No. 119, DOI: 10.1140/epje/s10189-023-00376-6.
(90) Menon, S. V. G.; Manohar, C.; Rao, K. S. A new interpretation of the sticky hard sphere model. *J. Chem. Phys.* **1991**, *95*, 9186−9190.
(91) Kabsch, W. xds. *Acta Crystallogr., Sect. D: Biol. Crystallogr.* **2010**, *66*, 125−132.
(92) Bliven, S.; Lafita, A.; Parker, A.; Capitani, G.; Duarte, J. M. Automated evaluation of quaternary structures from protein crystals. *PLoS Comput. Biol.* **2018**, *14*, No. e1006104.
(93) Krissinel, E.; Henrick, K. Inference of macromolecular assemblies from crystalline state. *J. Mol. Biol.* **2007**, *372*, 774−797.

https://doi.org/10.1021/acs.cgd.4c01535
Cryst. Growth Des. 2025, 25, 2418−2429